Journal of Magnetism and Magnetic Materials 321 (2009) 3813–3820

Contents lists available at ScienceDirect

Journal of Magnetism and Magnetic Materials

journal homepage: www.elsevier.com/locate/jmmm

Magnetic properties of Co-impregnated zeolites

P.G. Bercoff [a,*], H.R. Bertorello [a], C. Saux [b], L.B. Pierella [b], P.M. Botta [c], Toshiyuki Kanazawa [d], Ying Zhang [e]

[a] FaMAF, Universidad Nacional de Córdoba, and IFFAMAF, Conicet, Argentina
[b] CITeQ, Facultad Regional Córdoba, UTN, and Conicet, Argentina
[c] INTEMA, Conicet-UNMdP, Mar del Plata, Argentina
[d] JEOL USA, 11 Dearborn Road, Peabody MA 01960, USA
[e] Ames Laboratory, Materials Science and Engineering, Iowa State University, Ames IA 50011, USA

ARTICLE INFO

Article history:
Received 7 May 2009
Received in revised form
17 July 2009

PACS:
75.75.+a
82.75.Vx

Keywords:
Co–zeolite
Wet impregnation
Magnetic property
Cubic Co

ABSTRACT

The structure and magnetic properties of Co-containing zeolites prepared by wet impregnation were investigated. The samples were calcined and then reduced in flowing H_2. The samples studied have large saturation magnetization due to the presence of cubic Co particles over a wide range of sizes. The zero field cooling-field cooling curves show a sharp magnetization peak with a blocking temperature around 7 K followed by an exponential decay and two other peaks—of much lower amplitude—around 160 and 280 K. The low temperature peak is analyzed considering first, at T_{crit}, thermal relaxation toward equilibrium over an energy barrier, with increasing viscosity S with T. Above T_{crit} relaxation does not occur and viscosity abruptly goes to zero. The behavior of the smallest Co particles is unusual above the blocking temperature.

1. Introduction

Nowadays, nanoscale magnetism has great scientific interest and potential applications [1,2]. When the size of magnetic particles is reduced to a few nanometers, they often exhibit a number of outstanding physical properties such as giant magnetoresistance, superparamagnetism, large coercivity, as compared to the corresponding bulk values. Due to these unique physical properties upon size reduction, magnetic nanoparticles contribute to revolutionary changes in a variety of applications from biomedicine to spintronics [3,4]. In view of their technological importance, the synthesis of magnetic systems with characteristic nanoscale dimensions has attracted much attention in the research field.

The uniform intracrystalline microporosity of zeolites provides access to very large and well-defined surfaces with pore structures which can act as a convenient compartment for a desired reaction because, in many cases, they are able to induce size control and in other cases they form the species encapsulated in their cavities. Nowadays, there exists a considerable interest in the study of nanoparticles or nanoclusters of both metal oxides and other species, interacting with the lattice in micro- and mesoporous materials as they can be potentially used in optics, electronics, as sensors, as magnetic materials (small molecular magnets) and in photocatalysis [5,6]. Transition metal ion-containing molecular sieves are extensively investigated in academic and industrial laboratories because of their promising catalytic behavior in the oxidation of organic compounds and in the removal of NO_x [7–9]. In this respect, cobalt is an interesting transition metal ion, not only because of its promising catalytic activity, but also because of the rich spectroscopy of its divalent state [10].

In the case of zeolites of the type ZSM-5 (structure MFI: mirror framework inversion; Mobil five) the diameter of the channels is 0.51−0.56 nm [11]. A variety of Co species co-exists in Co–ZSM-5 prepared by ion-exchange or impregnation methods. Besides Co^{2+} and $(CoOH)^+$ at exchange sites, Co_3O_4 and Co oxo-ions have been detected in the zeolite channels and/or on the external surface of the zeolite microcrystals when the catalysts are heated in oxygen. These cobalt species may exhibit different catalytic properties [12,13].

On the other hand, cobalt–zeolites can be interesting materials not only as catalysts, but also because of their magnetic properties. Through different thermal treatments it is possible that the added cations keep their oxidation state or form different oxides or hydroxides. The structure of zeolites with pores or channels of well-defined size is particularly suitable for the study of magnetic properties of magnetic cations introduced into the structure

* Corresponding author. Tel.: +54 351 433 4051; fax: +54 351 433 4054.
E-mail address: bercoff@famaf.unc.edu.ar (P.G. Bercoff).

0304-8853/$ - see front matter © 2009 Elsevier B.V. All rights reserved.
doi:10.1016/j.jmmm.2009.07.046

[6,14]. In particular, when Co cations are introduced into the zeolite matrix by means of ionic interchange, the formation of superparamagnetic clusters of Co cations is observed, with blocking temperature below 7 K [14].

In this work, our aim is to study the magnetic properties of Co–zeolite with Co cations introduced via wet impregnation, calcined at 500 °C and reduced in H atmosphere. In this paper, we show how the Co is associated with the zeolite matrix and evaluate its magnetic response.

2. Experimental

ZSM-5 zeolite (MFI structure) with $Si/Al = 17$ ratio was synthesized by hydrothermal crystallization in a $Na_2O-Al_2O_3-SiO_2$ system using TPAOH (tetra-propyl ammonium hydroxide) as structure-directing agent by well-known methods [15] with some modifications. The template agent (TPA) was removed in N_2 flow (20 ml/min) from 110 to 520 °C at 10 °C/min and calcined in air at 520 °C for 12 h to obtain the Na–ZSM-5 zeolite. The ammonium form of the catalyst (NH_4–zeolite) was prepared by ion-exchange with 1 M NH_4Cl solution at 80 °C for 40 h. Co–HZSM-5 zeolites were prepared by wet impregnation of NH_4–MFI with aqueous solution of cobalt salt ($CoCl_2 \cdot 6H_2O$) to yield the desired wt% of the cation (2.8 Co wt%). Finally, the samples were reduced in flowing H_2 when heating from room temperature to 500 °C at 5 °C/min and holding at 500 °C for 5 h. The resulting samples were called Co2.8IR. The Co content was determined by atomic absorption.

Co distribution over the matrix was studied at low magnification with a LEO 1450 VP scanning electron microscope (SEM) and an energy dispersive spectrometer Genesis 2000. High magnification SEM micrographs in both secondary (SE) and transmission (STEM) modes and energy dispersive spectroscopy (EDS) were taken with JEOL JSM-7500F. The transmission electron microscopy (TEM) was performed on a FEI Tecnai G2 F20 field emission transmission electron microscope operated at 200 keV in both scanning and transmission modes, with high angle annular dark field (HAADF) detector for noticing *Z* contrast. Elemental analysis was performed using energy dispersive spectroscopy in STEM mode for point and line analysis. High resolution TEM (HRTEM) imaging mode has point to point resolution <0.25 nm and line to line resolution <0.10 nm.

Magnetic measurements were performed in a commercial SQUID (Quantum Design), varying the temperature from 5 to 300 K, with applied fields ranging from 0.0025 to 0.02 T, and at constant temperature with applied fields up to 5 T. Also, magnetization measurements as a function of time were carried out at selected constant temperatures with an applied field of 0.0075 T.

Crystal structure determinations were performed by means of X-ray diffraction patterns in a Philips diffractometer using CuKα radiation.

3. Results

3.1. Structural and microstructural characterization

The structural characterization of the prepared samples was previously published [16]. Here we mention only those aspects which are relevant to the magnetic properties.

X-ray diffractograms of the samples confirm the orthorhombic symmetry and crystallinity of the synthesized materials [16]. No Co oxides have been detected and metallic Co appears in a cubic phase, with mean crystallite size of 30 nm.

Fig. 1 shows the micrographs of sample Co2.8IR taken at 1.5 kx (top) and at 6 kx (middle). The bright spots correspond to Co particles of the order of 1−3 μm, as evidenced by the EDS spectrum taken on a bright spot (Point 1 in Fig. 1), where characteristic Co peaks are observed along with the Si, Al and O peaks corresponding to the matrix. The spectrum corresponding to Point 2 in Fig. 1 shows the characteristic energies of the matrix and very small peaks that correspond to Co energies.

Fig. 2 shows secondary (top) and backscattered (middle) electron images, SEI and BEI, respectively, taken at 150 kx. The blocky faceted grains are parallelepipeds with edges of

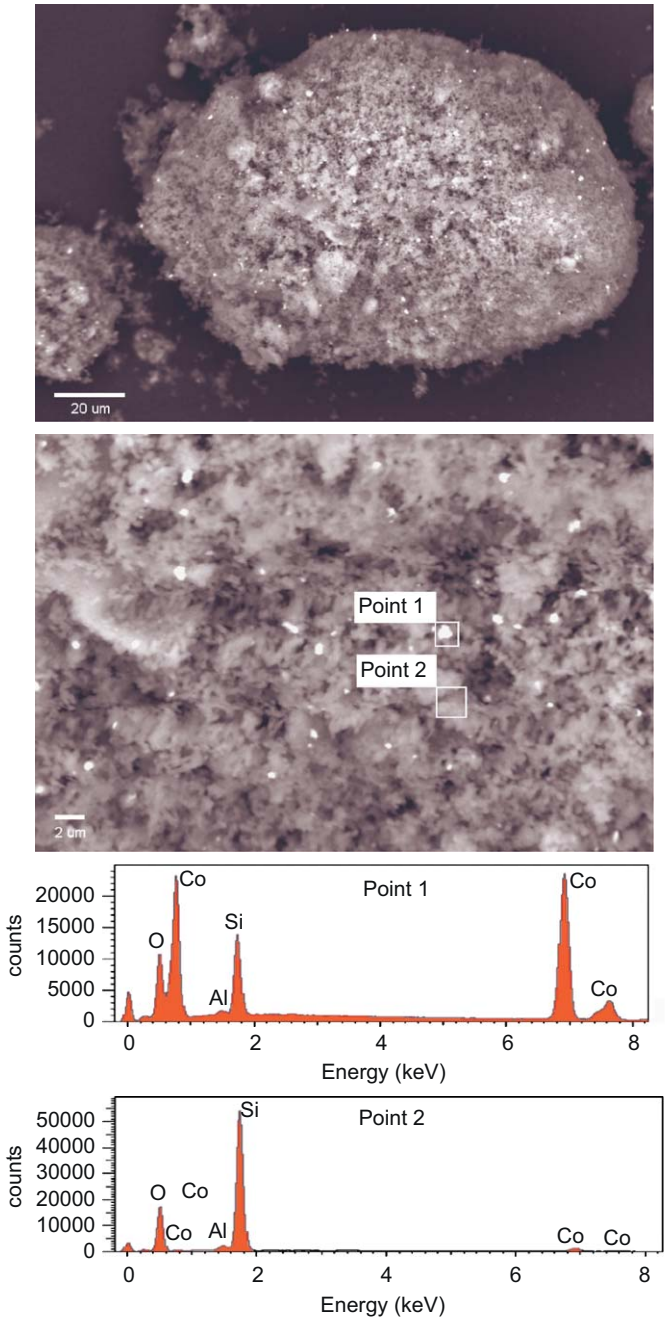

Fig. 1. Low magnification SEM micrographs. Top: 1.5 kx; the bar corresponds to 20 μm. Middle: 6 kx; the bar corresponds to 2 μm. The bright spots on the zeolite surface are Co particles; Point 1 marks a bright spot and Point 2 marks a dark zone. Bottom: EDS spectra corresponding to Points 1 and 2. Both the characteristic lines of Co (very intense) and the matrix are clearly seen in Point 1 spectrum, while the other shows the characteristic lines of the matrix and very small peaks of Co energies.

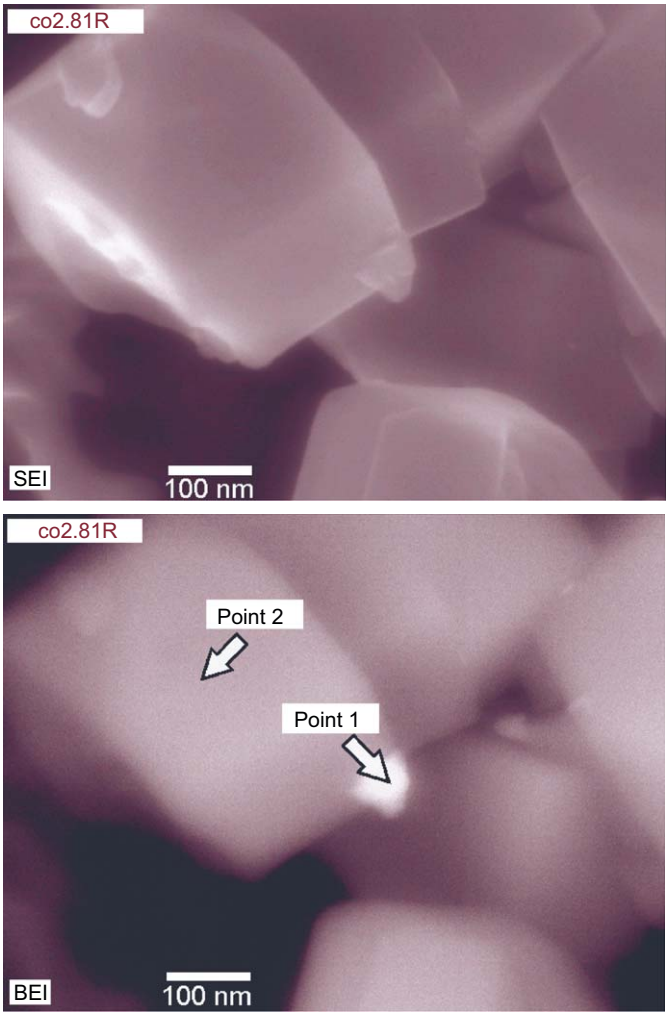

Fig. 2. SEI (top) and BEI (middle) taken at 150 kx. The bar corresponds to 100 nm. The EDS spectra at the bottom correspond to Points 1 and 2, respectively, indicated with white arrows in the BEI micrograph. The particle indicated in Point 1 is a Co particle and has a size of 60 nm.

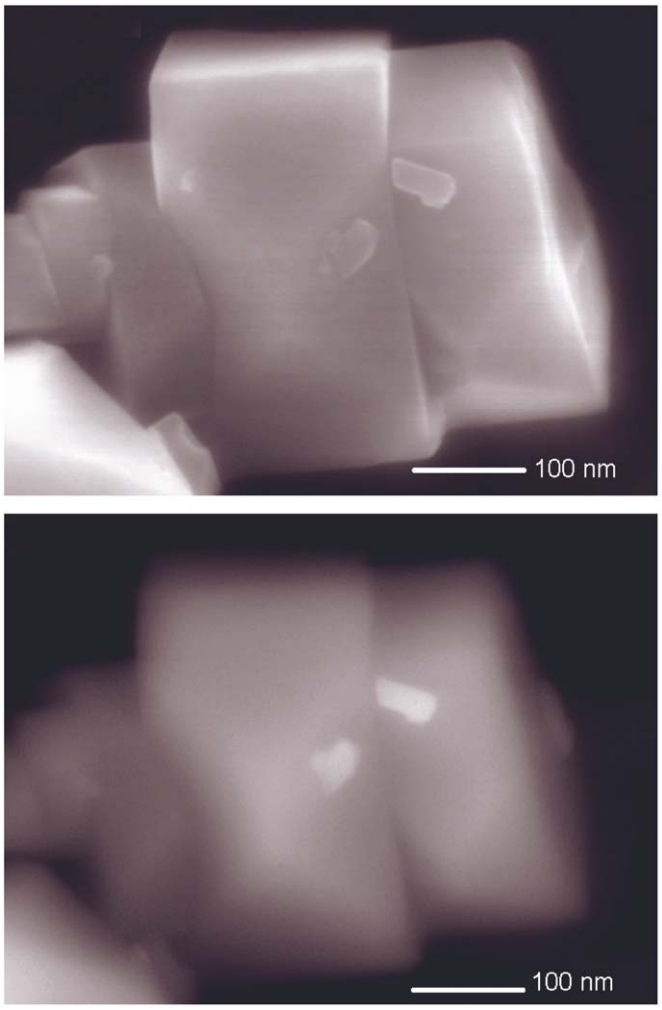

Fig. 3. SEI and BEI taken at 200 kx. The bar corresponds to 100 nm. The particles over the zeolite blocks are Co particles of around 25 nm and are noticed in the BEI micrograph.

approximately 300 nm and correspond to the zeolite matrix. The *Z* contrast in the BEI micrograph allows to identify small Co particles over the surface of the zeolite. The EDS spectra of Points 1 and 2 are shown at the bottom. In both spectra the characteristic peaks corresponding to the matrix are seen, but only in the spectrum obtained from Point 1 (where the bright spot is observed in BEI) intense characteristic Co peaks occur. This Co particle has a size of 60 nm. Associated with Point 2 there is only a very small signal from Co, indicating a low Co concentration in that position. Further comments will follow after the analysis of Fig. 5.

Fig. 3 shows Co particles of 25 nm on top of a zeolite particle, and the images of Fig. 4 (SEI, BEI and STEM from top to bottom) can resolve several Co particles of 10 nm, all of them on the surface of the zeolite grain.

High magnification TEM micrographs were taken in order to investigate the existence of Co particles smaller than 10 nm. Fig. 5a shows that there is a cluster of very fine metal particles, clearly not in the grains but on the surfaces (inside the marked square). The high magnification STEM image of Fig. 5b shows that the Co particles lie on the surface and are only a few nanometers across. This is the kind of particles which might originate the small Co peak observed in the spectrum corresponding to Point 2 in Fig. 2. Larger magnifications with TEM were not possible to achieve because the samples are quickly damaged by the electron beam.

In summary, Co was introduced in ZSM-5 via wet impregnation, heat-treatment and reduction in H atmosphere. Metallic Co is found in a wide range of particle sizes over the surface of the much larger zeolite particles. We have been able to detect groups

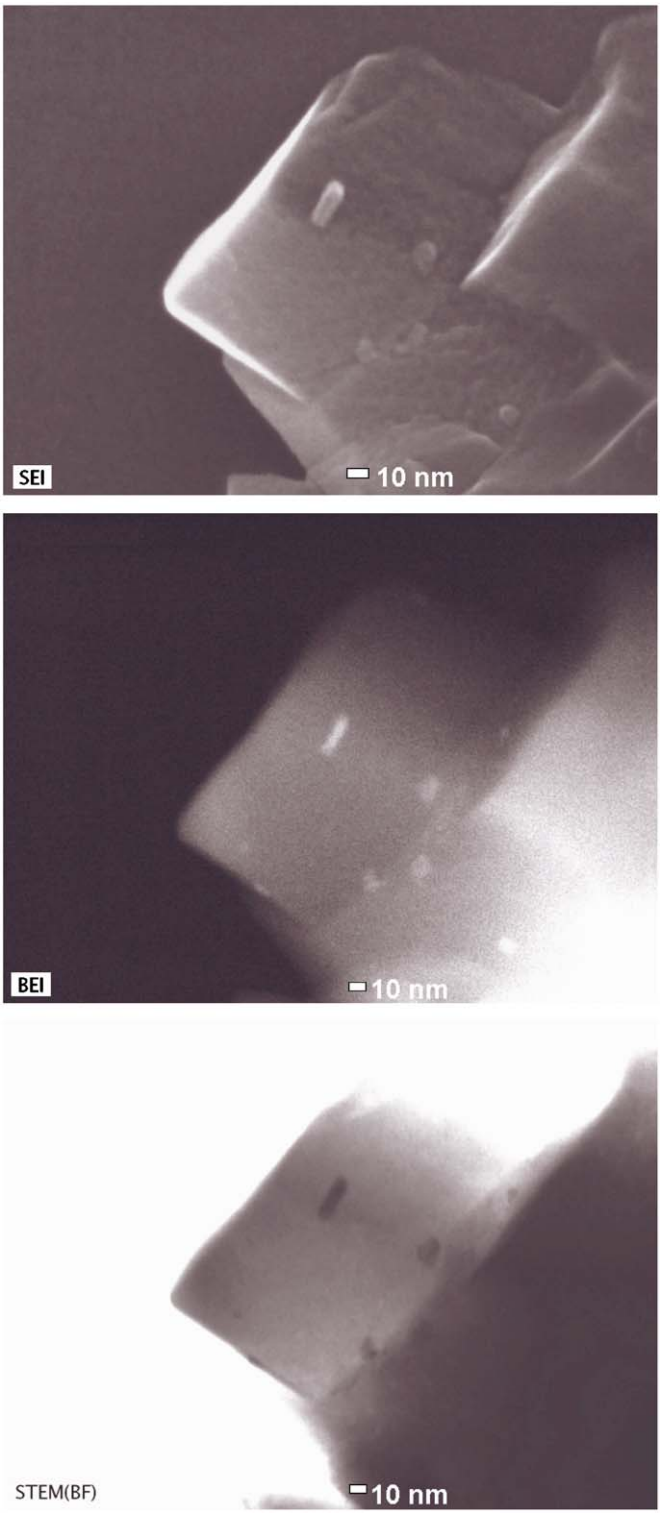

Fig. 4. SEI and BEI taken at 300 kx (top and middle). The bar corresponds to 10 nm. The bottom image is a scanning transmission electron micrograph (STEM) of the same portion as shown above.

of Co particles ranging 2−3 nm (Fig. 5b), 10−15 nm (Figs. 4 and 5a) and others of the order of 50 nm (Figs. 2 and 3). Also micron-sized particles of about 1–3 μm have been observed (Fig. 1). Although all the evidence indicates that Co is on the surface of the zeolite, it is not possible to disregard that within the zeolitic matrix small quantities of Co may be present, but are not resolved in the micrographs.

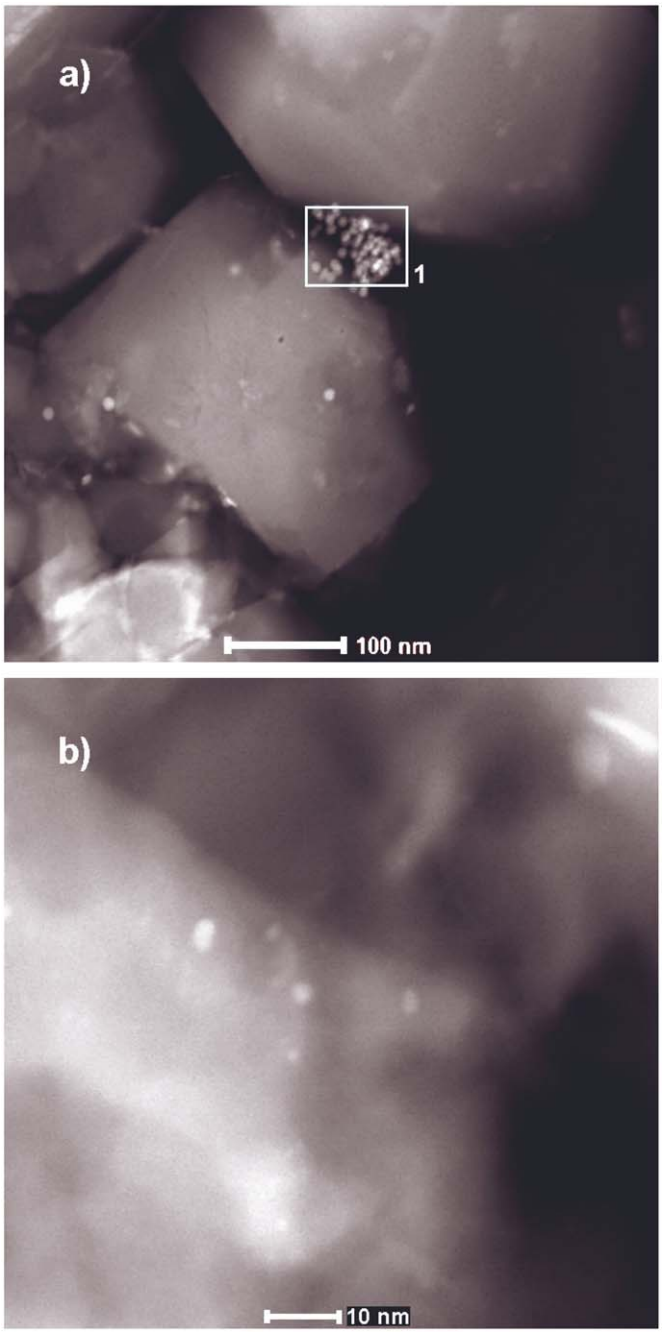

Fig. 5. (a) STEM image of a cluster of small Co particles. Bar = 100 nm. (b) STEM image (acquired with HAADF detector) of the smaller features of the studied sample. Particles smaller than 10 nm are noticed on the surface. Bar = 10 nm.

3.2. $M(T)$ and $M(H/T)$

Magnetization vs. temperature measurements were performed by means of the standard zero field cooling-field cooling (ZFC–FC) procedure with an applied field of 0.01 T.

Fig. 6 shows the ZFC–FC curves for sample Co2.8IR. The FC and ZFC curves do not coincide before 300 K. In the ZFC curve there is a sharp maximum at $T = 7$ K and two wider peaks around 160 and 280 K of much lower intensity (approximately 7% of the 7 K peak) which are hardly noticed in Fig. 6 due to the scale of the y axis. The inset in this figure shows an abrupt decrease of the first peak, which cannot be fitted either with Brillouin or with Langevin

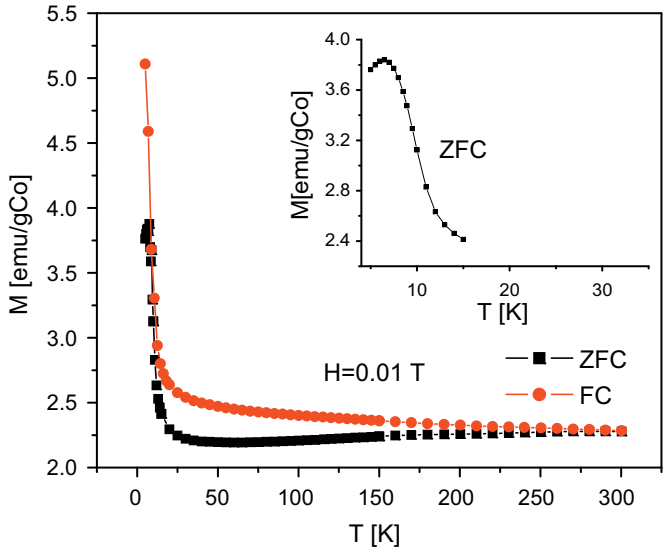

Fig. 6. ZFC–FC magnetization curves. The inset shows in detail the low temperature peak, with magnetization decreasing as $\exp(-T/T_1)$, with a decay constant $T_1 = 3.5$ K.

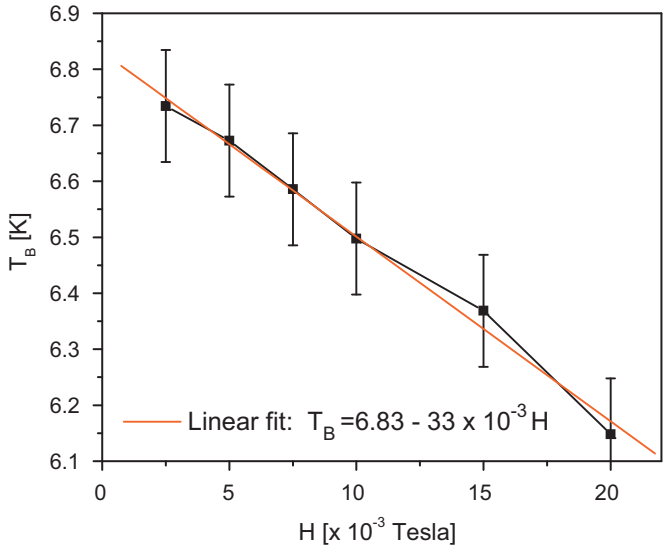

Fig. 7. Blocking temperature T_B as a function of the applied field H.

functions but an exponential of the type $\exp(-T/T_1)$, with a decay constant $T_1 = 3.5$ K. The largest contribution to the magnetization is a high ferromagnetic constant background, which is also observed at room temperature, due to large (micron-sized) ferromagnetic particles. The contribution of two different kinds of clusters is superimposed onto the background, with blocking temperatures of 160 and 280 K, corresponding to the broad maxima observed at these temperatures. The FC curve does not coincide with the ZFC curve from 10 K up to room temperature because of the ferromagnetic contribution of the micron-sized particles.

Measurements of the low-temperature peak in the ZFC curve were performed with different applied fields in order to study the blocking temperature dependence with the field. There is a decrease of the blocking temperature with increasing applied field (see Fig. 7). For $H = 0.1$ T the blocking temperature decreases below 5 K. A line can be fitted with these data and the corresponding analysis is left to the discussion section.

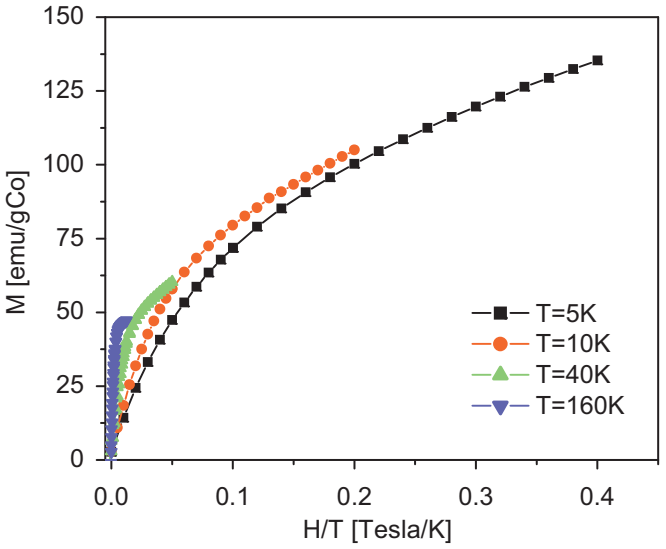

Fig. 8. M vs. H/T. No universal curve is found, due to several contributions to the magnetization.

Magnetization measurements at constant temperature were performed at 5, 10, 40 and 160 K.

The $M(H/T)$ experimental data do not converge to a universal curve (see Fig. 8) and the observed differences can be attributed to several clusters contributions that add up as the temperature increases. These contributions are due to the particle size distribution of cubic metallic Co.

3.3. $M(t)$

Some measurements of magnetization relaxation at low temperature were performed on the sample in order to clarify the nature of the low temperature peak observed in the $M(T)$-ZFC curve. All the relaxation measurements were performed after demagnetizing at 40 K, in the following modes:

(i) After ZFC from 40 K down to the selected temperature, a field of 0.0075 T was applied and $M(t)$ was registered (target temperature reached on cooling).
(ii) After ZFC from 40 K down to a temperature below 10 K, a field of 0.0075 T was applied. While measuring magnetization, the temperature was raised above 10 K at a rate of 2 K/min up to the selected temperature, where $M(t)$ was registered (target temperature reached on heating).
(iii) After FC with a field of 0.0075 T, from 40 K down to the selected temperature, $M(t)$ was measured (target temperature reached on cooling).
(iv) After FC with a field of 0.0075 T, from 40 K down to 5 K, the temperature was then raised up to the selected value and then $M(t)$ was measured (target temperature reached on heating).

The results of measurements (i) are shown in Figs. 9a and 10b, while measurements (ii) and (iii) are shown in Figs. 10a and 9b, respectively.

Some remarks are worth mentioning:

- ZFC, $T < 10$ K, measurements in mode (i), Fig. 9a: The relaxation expected over an energy barrier is observed. The total relaxation for a fixed time is higher at lower temperatures and consistent with the lowering of the "driving force" ($M - M_{eq}$) as we approach $T = 10$ K, where $M_{ZFC} = M_{FC}$. It may be

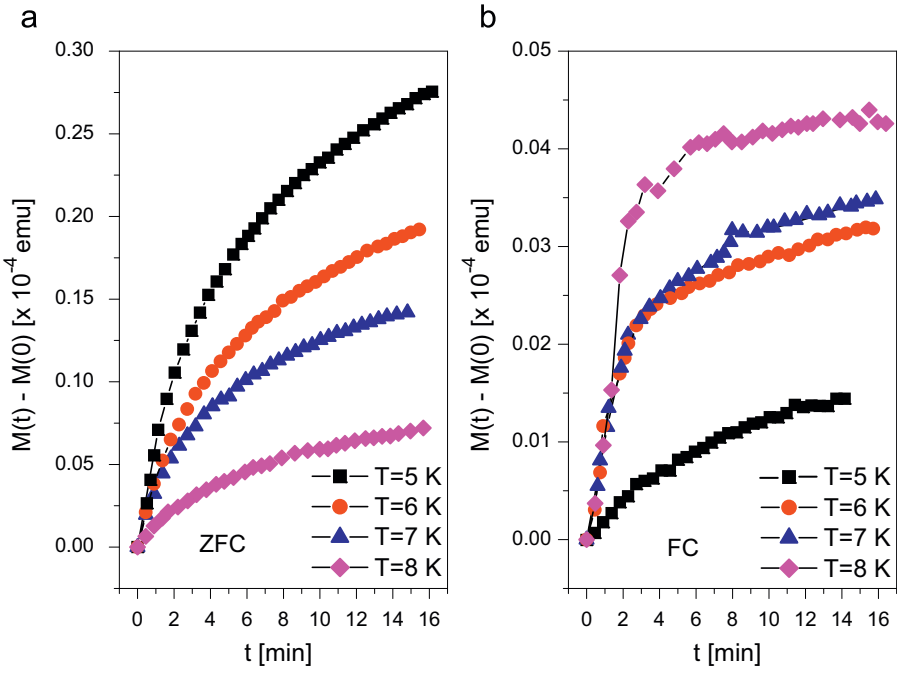

Fig. 9. M vs. t for different temperatures. (a) After ZFC in mode (i). (b) After FC in mode (iii).

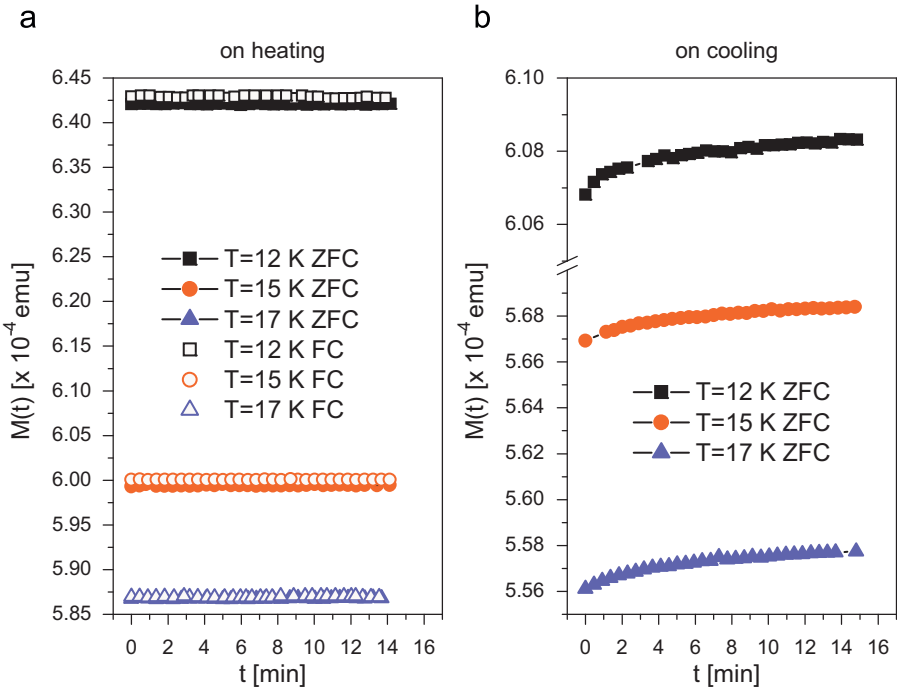

Fig. 10. M vs. t for sample Co2.8IR, for different temperatures, reached on heating (modes (ii) and (iv) in part (a)) and on cooling (mode (i) in part (b)).

noticed that the total relaxation in 15 min is 3–4% of the total relaxation needed to reach the equilibrium state. Initially, there is a fastest change of magnetization with time and after some minutes a $\ln(t)$ regime is reached.

- FC, $T<10$ K, measurements in mode (iii), Fig. 9b: The results are similar to those for ZFC measurements but a much smaller relaxation is observed, about $\frac{1}{20}$ of the value obtained for the ZFC relaxation. This is an indication that the equilibrium state is close to the measured value. Except for $T=5$ K, the relaxation occurs in two stages—the first one at a high rate which is completed in 2–3 min and the other one exhibits a similar behavior to that observed at 5 K in the ZFC measurements. We think this is due to an experimental effect, because the equipment took longer when trying to stabilize the temperature at 5 K and magnetization relaxed while the temperature stabilized, so that fast initial relaxation could not be recorded.
- ZFC and FC, $T>10$ K, measurements in modes (ii) and (iv), Fig. 10a: When the target temperature is reached on heating, both the ZFC and the FC measurements are coincident and do not

show any relaxation, which clearly means that the obtained states are the equilibrium ones. The same is observed for measurements in mode (iv), FC, for $T<10$ K, (not shown): in this case, no relaxation was observed for any temperature and the M values correspond to the $M(T)$-FC curve. This is the reason why we take the $M(T)$-FC curve (measured on heating) as the equilibrium curve $M_{eq}(T,H)$, for all temperatures.

- ZFC, $T>10$ K, measurements in mode (i), Fig. 10b: A relaxation is observed. The initial magnetization is about 95% of the equilibrium values observed in Fig. 10a. It is intriguing that the equilibrium value at $T>10$ K is reached instantly on heating but not on cooling.

4. Discussion and comments

According to the results obtained by XRD, EDS, Raman spectroscopy and TPR experiments (which confirmed the absence of cobalt oxide in the reduced samples) [16] we find that cubic Co is responsible for the high magnetization of the studied samples, amounting 135 emu/gCo at a field of 2 T and at 5 K. This value of M is close to the saturation magnetization value of cubic Co at 0 K (166 emu/g) [23].

The $M(T)$-ZFC curve (Fig. 6) shows a prominent feature—the appearance of a well-defined magnetization peak at low temperature followed by an exponential decay. The small width of this peak indicates that the size distribution of the particles which originate it is also narrow. The contribution of this peak to the total magnetization is comparable to the background, indicating that there is a very large number of the smaller particles that are responsible for this peak. Two smaller peaks are also observed at around 160 and 280 K, which we assign to cubic Co particles of larger size.

In Fig. 11, part (a) shows the low temperature peak appearing in the ZFC curve, after background subtraction. The background is constant and produced by other ferromagnetic contributions due to large particles of cubic Co. Part (b) shows dM/dT, where the blocking temperature T_B is defined as the temperature where $dM/dT=0$, and the temperature T_{crit} where $d^2M/dT^2=0$.

We consider that two processes take place at low temperature, which give rise to this peak:

(1) For temperatures $T<T_{crit}$ the obtained states in ZFC experiments are not equilibrium states (see Fig. 9a) but evolve toward the equilibrium state with magnetization $M_{eq}(T,H)$ given by the FC measurements. It is this process that produces a blocking temperature T_B.
(2) For $T>T_{crit}$ the obtained states in ZFC experiments are equilibrium states (see Fig. 10a). The magnetization of the particles which originate this peak decreases exponentially with T, down to $M_{eq}=0$.

Both types of behavior are clearly distinguished when plotting dM/dT as a function of temperature, as shown in Fig. 11, for an applied field $H=0.0075$ T.

The ZFC–FC curves depend on the magnetic relaxation and the magnetization is the result of cumulated relaxation effects up to the time when the magnetization is measured at temperature T.

The observed relaxation both in the ZFC and in the FC measurements is neither purely exponential nor logarithmic in time—there is an initial fast relaxation that is completed in 3–4 min and a $\ln(t)$ behavior is observed afterwards. We think this is due to the existence of non-interacting particles with some particle-size distribution. Considering the narrow peak observed in the ZFC curve, this distribution must also be narrow. In the limit $H \ll H_a$, H_a being the anisotropy field, the definition of the

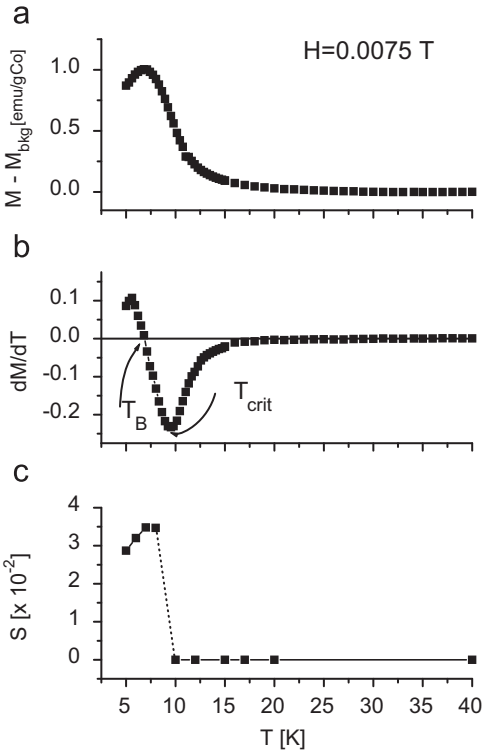

Fig. 11. $M(T)$ vs. T and dM/dT vs. T, ZFC curve. (a) $M(T)$ corresponding to the low temperature peak after background substraction. (b) dM/dT, where the blocking temperature T_B is defined as the temperature where $dM/dT=0$ and the temperature T_{crit} where $d^2M/dT^2=0$. (c) Viscosity constant $S(T)$.

magnetic viscosity which is independent from the initial and final states is [27]

$$S=-\frac{1}{M_0-M_{eq}}\frac{dM}{d(\ln(t))}, \tag{1}$$

where $M_0=M(T,H)$ is the value of magnetization at the beginning of the relaxation process and $M_{eq}(T,H)$ is the final state.

Using the results given in Figs. 9a and 10a, S values are calculated for the ZFC measurements with Eq. (1) and are plotted in Fig. 11c. For $T<T_B$ the behavior of S vs. T is similar to the results observed for ferritin protein samples [28] and α–Fe_2O_3 particles [29]. For $T>T_{crit}$ the magnetic viscosity vanishes, demonstrating that the achieved states are indeed equilibrium states.

It can be seen that the magnetic viscosity S rises monotonically with temperature for $T<T_{crit}$. This is consistent with the assumption that relaxation is produced by thermal activation over an energy barrier.

At $T=T_{crit}$ an abrupt change toward $S=0$ occurs and for $T>T_{crit}$, no relaxation is observed. The measured magnetization is fitted by

$$M(T,H)=M_0\exp(-T/T_1), \tag{2}$$

T_1 being a decay constant. This behavior differs from a Curie-type law, which would correspond to paramagnetic particles, and needs further study.

The appearance of a blocking temperature T_B is interpreted as thermal activation over an energy barrier. In the low applied field approximation, the energy barrier that the magnetic system must overcome by thermal activation is

$$\Delta E=K_1V-MH, \tag{3}$$

K_1 being the anisotropy constant, V the volume, M the total magnetization of volume V and H the applied field.

Then, when the relaxation is produced by thermal activation over an energy barrier given by Eq. (3), using that $\Delta E \approx 25 k_B T_B$ [25], where k_B is Boltzmann constant, the following relation can be obtained:

$$T_B = \frac{K_1 V}{25 k_B} - \frac{M}{25 k_B} H. \quad (4)$$

From the fitting of the experimental data of T_B vs. H (Fig. 7) the slope and y intercept can give us K_1V and M. We estimated the value of V by considering the responsible of this low-temperature behavior is cubic Co. We were led to this by the evidence given in the previous characterization study [16] and the results of Section 3.1. So, if we use the atomic volume of Co $v_{at} = 1.11 \times 10^{-29}\,\mathrm{m^3/at}$ and the number of Bohr magnetons per atoms for the metallic state of Co $n_0 = 1.714\,\mu_B$/at [23] we end up with 869 atoms per cluster ($V = 9.6 \times 10^{-27}\,\mathrm{m^3}$; $d \sim 2.6\,\mathrm{nm}$). With these values, and using the independent term of Eq. (4), we find $K_1 \sim 3 \times 10^5\,\mathrm{J/m^3}$. This anisotropy is somewhat lower than the value expected for bulk metallic Co ($5.3 \times 10^5\,\mathrm{J/m^3}$ [23]), but we must keep in mind that here we are dealing with small volume clusters, in which the ratio of atoms at the surface with respect to the bulk is very high and this leads to canting of atomic magnetic moments at the surface, thus reducing magnetic anisotropy. This effect has already been observed in different systems of nanometric particles [26]. It is remarkable that in our case such small particles are not superparamagnetic above T_B.

From the blocking temperatures that correspond to the peaks of 160 and 280 K we estimate the sizes of the particles that originate these peaks. The result is $d_{160} \sim 7$ nm and $d_{280} \sim 9$ nm for the lower and higher temperatures, respectively.

The larger particles that are visible in our SEM micrographs have sizes of the order of 1 μm and their blocking temperature is above room temperature. These bigger particles are responsible of the high magnetization background observed in the FC–ZFC curves, which is still present at room temperature.

A point that needs clarification is why the FC curve measured on heating gives the magnetization equilibrium values instantly, although this is not true on cooling. The reason would certainly be related to a strong dependence of the energy barrier landscape on the temperature.

5. Conclusions

The magnetic behavior of Co impregnated ZSM-5 zeolites was studied. Reduced samples were prepared and their magnetic properties were measured as a function of temperature and applied magnetic field.

Co particles were detected by SEM and TEM with a significant size distribution, which are responsible for the different magnetic contributions. We observed that micron-sized particles of metallic Co are responsible for the high observed values of saturation magnetization and nanoparticles of ~2.6 nm give rise to a large magnetic contribution at low temperature, which is not superparamagnetic in nature. Larger nanometric particles with particle size of the order of 10 nm make a smaller contribution at higher temperatures. Particles larger than 15 nm have blocking temperature above room temperature and contribute to the large ferromagnetic background. A magnetization peak is observed in the ZFC curve, which is interpreted as the result of two relaxation mechanisms: below T_{crit} a relaxation toward M_{eq} given by the FC curve and governed by a thermal activation over an energy barrier. Above T_{crit} an exponential dependence of $M(T)$ toward $M_{eq} = 0$ is observed. This is consistent with a spin reorientation mechanism.

Acknowledgments

This work was partially funded by Consejo Nacional de Investigaciones Científicas y Técnicas (CONICET), Argentina, PIP no. 6452 and PIP no. 6313/05; Agencia Nacional de Promoción Científica y Tecnológica, Argentina, PICT no. 12-14657; Secretaría de Ciencia y Tecnología, Universidad Nacional de Córdoba, Argentina; UTN-PID 25E092; the Ministry of Science and Education of Spain (MEC) under Project MAT 2004-05130-C02-01. The work at the Ames Laboratory was supported by the Department of Energy, Office of Basic Energy Sciences, under Contract no. DE-AC02-07CH11358. P.G. Bercoff is indebted to M.J. Kramer, from Ames Laboratory, for his invaluable help with TEM/STEM images.

References

[1] B. Barbara, Solid State Sci. 7 (2005) 668.
[2] K.M. Krishnan, A.B. Pakhomov, Y. Bao, P. Blomqvist, Y. Chun, M. Gonzales, K. Griffin, X. Ji, B.K. Roberts, J. Mater. Sci. 41 (2006) 793.
[3] R. Hergt, S. Dutz, R. Müller, M. Zeisberger, J. Phys. Condens. Matter 18 (2006) S2919.
[4] S. Parkin, X. Jiang, C. Kaiser, A. Panchula, K. Roche, M. Samant, Proc. IEEE 91 (2003) 661.
[5] J.A. Rabo, Appl. Catal. A Gen. 229 (2002) 7.
[6] E.M. Barea, V. Fornes, A. Corma, P. Bourgues, E. Guillon, V.F. Puntes, Chem. Commun. 1974 (2004).
[7] D.L. Vanoppen, P.A. Jacobs, Catal. Today 49 (1999) 177.
[8] A. Corma, H. Garcia, Chem. Rev. 103 (2003) 4307.
[9] Y. Li, J.N. Armor, Appl. Catal. B 5 (1995) L257.
[10] A. Verberckmoes, Microp. Mesop. Mater. 22 (1998) 165.
[11] W.M. Meier, D.H. Olson, Atlas of Zeolite Structure Types, Butterworth-Heinemann, USA, 1992.
[12] C. Lee, P. Chong, Y. Lee, C. Chin, L. Kevan, Microp. Mater. 12 (1997) 21.
[13] X. Wang, H. Chen, W.M.H. Sachtler, Appl. Catal. B Environ. 29 (2001) 47.
[14] H.R. Bertorello, L.B. Pierella, P.G. Bercoff, C. Saux, J.P. Sinnecker, Physica B 354 (2004) 137.
[15] P. Chu, U.S. Patent 3.709.979, 1972.
[16] L.B. Pierella, C. Saux, H.R. Bertorello, P.G. Bercoff, P.M. Botta, J. Rivas, Mater. Res. Bull. 44 (2009) 1036.
[23] R.M. Bozorth, Ferromagnetism, IEEE Press, New York, 1993.
[25] A.H. Morrish, The Physical Principles of Magnetism, IEEE Press, New York, 2001, p. 362.
[26] O. Iglesias, A. Labarta, Physica B 343 (2004) 286;
S. Mørup, J. Magn. Magn. Mat 266 (2003) 110.
[27] E.M. Chudnovsky, J. Tejada, Macroscopic quantum tunneling of the magnetic moment, in: Cambridge Studies in Magnetism, Cambridge University Press, Cambridge, 1998.
[28] J. Tejada, X.X. Zhang, J. Phys. Cond. Matt. 6 (1994) 263.
[29] E. Vincent, J. Hamman, P. Prene, E. Tronc, J. Phys. 4 (1994) 273.